Effect of spin-orbit coupling on magnetoresistance in organic semiconductors

Y. Sheng,[1] T. D. Nguyen,[1] G. Veeraraghavan,[2] Ö. Mermer,[1] and M. Wohlgenannt[1,*]

[1]*Department of Physics and Astronomy and Optical Science and Technology Center, University of Iowa, Iowa City, Iowa 52242-1479, USA*

[2]*Department of Electrical and Computer Engineering and Optical Science and Technology Center, University of Iowa, Iowa City, Iowa 52242-1595, USA*

(Received 17 July 2006; revised manuscript received 2 October 2006; published 2 January 2007)

We study the recently discovered organic magnetoresistance (OMAR) effect in a pair of materials that have similar chemical structures except that one contains a heavy atom to enhance spin-orbit coupling. We use photoluminescence spectroscopy to estimate the spin-orbit coupling strength. In the material with weak spin-orbit coupling the characteristic magnetic field scale is comparable to the hyperfine coupling strength. In the material with strong spin-orbit coupling we find that the OMAR is strongly reduced in size and the OMAR traces clearly exhibit a second, higher field scale which we identify with the spin-orbit coupling strength. We model our results using the standard spin-dynamics Hamiltonian.

DOI: 10.1103/PhysRevB.75.035202 PACS number(s): 73.50.−h, 73.43.Qt

I. INTRODUCTION

There has been growing interest in magnetoelectronic effects[1–6] in organic semiconductors. We recently discovered[1] a large, low-field (up to 10% at 10 mT and 300 K) magnetoresistive effect in organic light-emitting diodes (OLEDs), which we dubbed organic magnetoresistance (OMAR). The effect has also been observed by others.[6] In addition to its potential applications, OMAR poses a significant scientific puzzle since it is, to the best of our knowledge, the only known example of large room-temperature magnetoresistance in nonmagnetic materials with the exception of high-mobility materials.[7,8]

To the best of our knowledge the mechanism causing OMAR is currently not known with certainty, although two theories based on spin dynamics have been suggested very recently.[6,9] In general, magnetoresistance in nonmagnetic devices can be caused by several different physical principles: (i) Lorentz force deflection, causing effects like Hall voltages, classical magnetoresistance, and extraordinary magnetoresistance,[10] (ii) quantum-mechanical diamagnetism, such as effects associated with Landau levels or hopping magnetoresistance,[11] (iii) interference phenomena such as weak localization[12] that are sensitive to magnetic fields because the vector potential enters the Schrödinger equation in a way that leads to phase shifts, and finally (iv) spin dynamics. In our opinion, we have been able to exclude (i)–(iii) in our earlier work[3] as possible explanations for OMAR. However, spin dynamics could be the cause of OMAR. Prior work[6,13] has shown that OMAR is substantially reduced upon introduction of spin-orbit coupling. No attempt was made, however, to examine on a quantitative level whether this observation can actually be derived from the spin-orbit coupling Hamiltonian. In any case, a detailed comparison between theory and experiment would not have been possible, because experimental OMAR traces in Refs. 6 and 13 in materials with strong spin-orbit coupling were below the experimental noise level. In the present work we remedy these shortcomings by using a modulation technique to record OMAR traces in materials with strong spin-orbit coupling.

For the benefit of the reader, we will briefly summarize some of the main experimental results regarding OMAR. We have shown[1–3,14] that (i) OMAR is a bulk effect rather than an interface effect; (ii) the functional form of OMAR is accurately described by the laws $B^2/(B^2+B_0^2)$ or $B^2/(|B|+B_0)^2$ dependent on the material, where $B_0 \approx 5$ mT in all materials we have studied; (iii) the effect is independent of the magnetic field direction; (iv) the magnitude of the OMAR effect is only weakly dependent on the minority carrier density; and (v) OMAR can be of positive or negative sign, dependent on material and/or operating conditions of the devices.

II. EXPERIMENT

The device fabrication steps were described in detail in our earlier publications[1–3] and follow the standard OLED fabrication recipe. The π-conjugated small molecules tris(8-hydroxyquinoline) aluminium (Alq_3) and tris(2-phenylpyridine)iridium [$Ir(ppy)_3$] were purchased from H. W. Sands corporation. The samples were mounted on the cold finger of a closed-cycle helium cryostat located between the poles of an electromagnet. The magnetoconductance ratio $\Delta I/I$, for the Alq_3 devices was determined by measuring the current I at a constant applied voltage V for different magnetic fields, B. Due to the much smaller magnetoresistance effect in $Ir(ppy)_3$ devices, $\Delta I/I$ could not be measured in the same way. Instead, a modulation method was required: for each constant voltage and B, $I(t)$ pulses are recorded as the applied magnetic field is switched on and off multiple times at a frequency of approximately 1 Hz. The ratio $\Delta I/I$ for that certain magnetic field is calculated using fast fourier transform (LABVIEW) from the current pulses. By varying the applied magnetic field, $\Delta I/I$ as a function of B is obtained. The number of pulses was chosen such that a sufficient signal-to-noise ratio was achieved. The modulation technique employed required the usage of a relatively small magnet ($B < 300$ mT) since larger magnets have large self-inductance, severely limiting the achievable modulation frequency. For

 ©2007 The American Physical Society

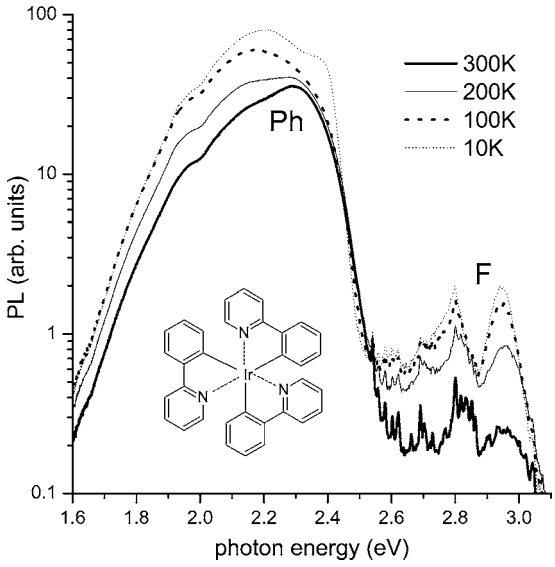

FIG. 1. The photoluminescence of $Ir(ppy)_3$ at different temperatures. The emission bands due to fluorescence (F) and phosphorescence (Ph) are assigned.

the photoluminescence (PL) measurements, films of about 100 nm thickness were spin coated from a chloroform solution onto a glass substrate. The uv lines (364 and 357 nm) from an argon ion laser (about 200 mW) were used to excite the samples. PL emission was collected and spectrally resolved using an Ocean Optics USB-2000UV spectrometer.

III. EXPERIMENTAL RESULTS

A. Fluorescence and phosphorescence spectra

Before studying the effect of spin-orbit coupling introduced by the heavy atom in $Ir(ppy)_3$ on OMAR, we want to document and assess its spin-orbit coupling strength using PL. Figure 1 shows the PL of $Ir(ppy)_3$ at different temperatures. The emission bands due to fluorescence (F) and phosphorescence (Ph) are assigned.[15–17] In Sec. IV A we will use the measured spectra to estimate the spin-orbit coupling strength.

B. OMAR in materials with different spin-orbit coupling strengths

Figures 2 and 3 show the measured OMAR effect in ITO/PEDOT/Alq_3/Ca and ITO/PEDOT/$Ir(ppy)_3$/Ca devices, at different voltages and different temperatures (ITO is indium tin oxide). These materials were chosen because of their similar chemical structure except for the Ir atom which introduces strong spin-orbit coupling. The results in Alq_3 are described in more detail elsewhere.[2] The behavior of OMAR in Alq_3 and $Ir(ppy)_3$ devices differs dramatically: the magnitude of OMAR in $Ir(ppy)_3$ is roughly two orders of magnitude smaller than that in Alq_3. Moreover, it is evident that the OMAR traces in $Ir(ppy)_3$ are comprised of a low-field and a high-field effect of opposite signs. In terms of a possible analysis of the $Ir(ppy)_3$ data this behavior implies that there are at least two relevant coupling strengths in materials with

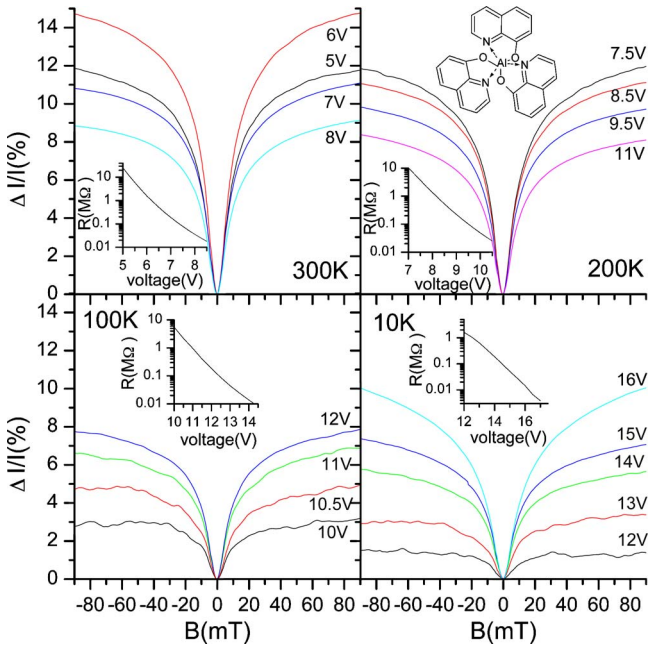

FIG. 2. (Color online) Magnetoconductance $\Delta I/I$ curves, measured in an ITO/PEDOT/Alq_3 ($\approx$100 nm)/Ca device at different voltages and different temperatures. The insets show the device resistance as a function of the applied voltage.

strong spin-orbit coupling, in contrast to Alq_3, where only a single coupling strength is evident. It appears natural to assign the second coupling strength in $Ir(ppy)_3$ to the spin-orbit coupling. We note that, since the $Ir(ppy)_3$ device also contains a second organic material, namely, PEDOT, it is conceivable the the weaker cone could be caused by the PEDOT layer. Upon further consideration this appears unlikely, since the resistance of the PEDOT layer is negligible compared to that of $Ir(ppy)_3$. Nevertheless, in a control experiment we have measured devices without PEDOT, and still observed both cones, where the smaller cone increases in magnitude with decreasing temperature. The results including the PEDOT layer are shown because of their higher signal-to-noise ratio.

IV. DISCUSSION

A. Extraction of the intersystem crossing rate from the photoluminescence spectra

It is well known that in organics the fluorescence (phosphorescence) band originates from the radiative recombination of singlet (triplet) excitons. Moreover, photoexcitation results almost exclusively in the formation of singlets. Therefore, quite generally, the relative strength of the fluorescence and phosphorescence bands depends on the intersystem crossing rate k_{ISC} which in turn is intimately related to the spin-orbit coupling strength.[20] It can be readily shown from the rate equations for singlet and triplet excitons (such equations contain radiative and nonradiative recombination and intersystem crossing terms) that the ratio between triplet emission flux P and singlet emission flux F is given by

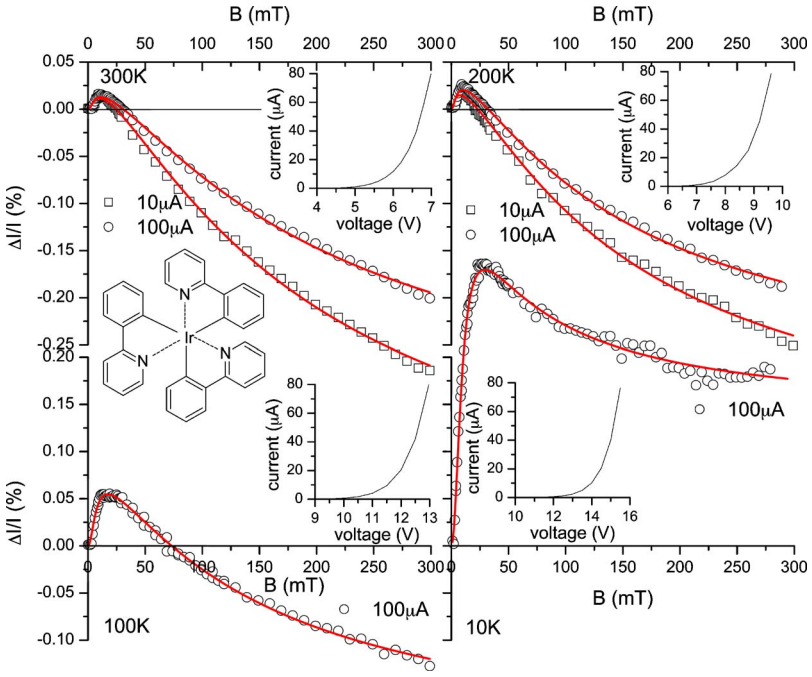

FIG. 3. (Color online) Magnetoconductance $\Delta I/I$ curves measured in an ITO/PEDOT/Ir(ppy)$_3$ ($\approx$100 nm)/Ca device at different voltages and different temperatures. The insets show the device resistance as a function of the applied voltage.

$$\frac{P}{F} = \frac{I_P/\hbar\omega_P}{I_F/\hbar\omega_F} = k_{ISC}\tau_S^* \frac{\eta_P}{\eta_F}, \tag{1}$$

where I_P and I_F are the phosphorescence and fluorescence intensity, respectively; $\hbar\omega_P$ and $\hbar\omega_F$ are the phosphorescence and fluorescence photon energy, respectively; τ_S^* is the singlet lifetime without considering the intersystem crossing rate and is given by

$$\tau_S^* = \frac{1}{k_{R,S} + k_{NR,S}}. \tag{2}$$

$k_{R,S}$ ($k_{NR,S}$) is the radiative (nonradiative) singlet recombination rate. η_F and η_P are the singlet and triplet emission quantum efficiencies. Equation (1) contains two unknowns, and to be able to extract k_{ISC} from the (spectrally integrated) phosphorescence and fluorescence intensities we need to make an assumption regarding η_P/η_F. Since the emission efficiency of Ir(ppy)$_3$ can certainly compete with the best fluorescent materials,[17] we therefore expect that $\eta_P/\eta_F \approx 1$ (the $\approx$ sign reflects an order of magnitude estimate). For τ_S^*=14 ns we used the experimental value for Alq$_3$,[18] which has a similar chemical structure to Ir(ppy)$_3$. The k_{ISC} values extracted from the photoluminescence spectra Fig. 1 are given in Table I. Table I also contains the corresponding Zeeman field B_{ISC} determined from the uncertainty relationship $E_{Zeeman}/k_{ISC} = \hbar/2$ (see next section), with $E_{Zeeman} = g\mu_B B_{ISC}$. The table also shows that k_{ISC} is approximately independent of temperature, in agreement with expectations based on spin-orbit coupling as the origin of the intersystem crossing.

B. Theoretical part: Modeling the spin dynamics induced by hyperfine and spin-orbit coupling

Here we will study whether the experimental results in Sec. III B are consistent with expectations based on spin dynamics induced by hyperfine and spin-orbit coupling. This theoretical part is motivated, in part, by two observations. (i) Prigodin *et al.*[6] and Hu *et al.*[13] have shown that the magnitude of OMAR decreases dramatically in materials with strong spin-orbit coupling, suggesting that OMAR is caused by spin dynamics. (ii) We have previously shown[14] that the functional dependence $B^2/(B^2+B_0)^2$ that OMAR obeys in some materials can be readily derived from the spin dynamics induced by the standard hyperfine Hamiltonian. In particular, we have shown that if one calculates the time average of the expectation value of the z component of the spin operator, $\overline{S_z}$, then the law $B^2/(B^2+B_0)^2$ follows naturally. The motivation for studying this particular quantity is taken from the two theories of OMAR that have recently been developed.[6,9] In these theories, spin dynamics enters through the relative spin orientation of charge pairs that participate in spin-dependent recombination[6] or spin-dependent hopping,[9] and we therefore expect that $\overline{S_z}$ is indeed the relevant quantity (see Ref. 14).

1. Spin-orbit coupling

The calculation for the hyperfine Hamiltonian that applies to materials with weak spin-orbit coupling can be found in Ref. 14 and will not be repeated here. The standard spin-orbit coupling Hamiltonian for a single electron is given by

TABLE I. Values for the intersystem crossing rate k_{ISC} and the corresponding Zeeman field B_{ISC} in Ir(ppy)$_3$ extracted from the photoluminescence spectra (see Fig. 1) using Eq. (1).

Temperatrue (K)	k_{ISC} (s^{-1})	B_{ISC} (mT)
300	2×10^{10}	100
200	1×10^{10}	60
100	1×10^{10}	60
10	1×10^{10}	60

$$\hat{H}_{SO} = \omega_0 \left(\frac{g_L}{g_S} \hat{L}_z + \hat{S}_z \right) + \frac{b}{\hbar} \hat{\vec{L}} \hat{\vec{S}}, \tag{3}$$

where g_L and g_S are the orbital and spin g factors, respectively, which we will assume to be equal to 1 and 2, respectively, from now on. $\vec{L}$ ($\vec{S}$) is the electronic orbital (spin) angular momentum. We assume $l=1$ for simplicity; however, in reality it is $l=2$ that applies to the materials used in this study. b is the spin-orbit interaction strength. $\omega_0 = g_S \mu_B B/\hbar$, where μ_B is the electronic Bohr magneton. The Hamiltonian will be written in matrix form where we use the following basis vectors: $|\uparrow\Uparrow\rangle$, $|\leftrightharpoons\Uparrow\rangle$, $|\downarrow\Uparrow\rangle$, $|\uparrow\Downarrow\rangle$, $|\leftrightharpoons\Downarrow\rangle$, and $|\downarrow\Downarrow\rangle$. The single-barb arrow denotes the z component of the orbital momentum, whereas the open-font arrow denotes the spin. We
obtain the following result:

$$\hat{H}_{SO} = \hbar \begin{bmatrix} \omega_0 + b/2 & 0 & 0 & 0 & 0 & 0 \\ 0 & \omega_0/2 & 0 & \sqrt{2}b/2 & 0 & 0 \\ 0 & 0 & -b/2 & 0 & \sqrt{2}b/2 & 0 \\ 0 & \sqrt{2}b/2 & 0 & -b/2 & 0 & 0 \\ 0 & 0 & \sqrt{2}b/2 & 0 & -\omega_0/2 & 0 \\ 0 & 0 & 0 & 0 & 0 & -\omega_0 + b/2 \end{bmatrix}. \tag{4}$$

It is evident that $\hat{H}_{SO}$ can be separated into four invariant subspaces spanned by $|\uparrow\Uparrow\rangle$, $\{|\leftrightharpoons\Uparrow\rangle, |\uparrow\Downarrow\rangle\}$, $\{|\downarrow\Uparrow\rangle, |\leftrightharpoons\Downarrow\rangle\}$, and $|\uparrow\Downarrow\rangle$. Using the procedure in Ref. 14, we obtain the following result for subspace $\{|\leftrightharpoons\Uparrow\rangle, |\uparrow\Downarrow\rangle\}$ (in units of $\hbar/2$):

$$\overline{S_z} = \frac{(\omega_0 + b)^2}{(\omega_0 + b)^2 + 8b^2}. \tag{5}$$

The result Eq. (5) is not symmetric about $\omega_0=0$, because the two levels in the subspace are split by an energy $b/2$ even at zero field. Dependending on the signs of b and ω_0, applying an external field can reduce or increase this level splitting. However, averaging over all spin orientations removes this offset and yields

$$\overline{S_z} = \frac{\omega_0^2}{\omega_0^2 + 8b^2} \tag{6}$$

2. Combined spin-orbit and hyperfine coupling

Finally, we consider the combined Hamiltonian

$$\hat{H}_{SOHF} = \omega_0 \left(\frac{g_L}{g_S} \hat{L}_z + \hat{S}_z \right) + \frac{a}{\hbar} \hat{\vec{S}} \hat{\vec{I}} + \frac{b}{\hbar} \hat{\vec{L}} \hat{\vec{S}}, \tag{7}$$

where a is the hyperfine coupling constant and $\vec{I}$ is the proton spin. Upon writing out the 12×12 Hamiltonian matrix we find that it can be separated into five invariant subspaces spanned by $|\uparrow\Uparrow\uparrow\rangle$, $\{|\leftrightharpoons\Uparrow\uparrow\rangle, |\uparrow\Downarrow\uparrow\rangle, |\leftrightharpoons\Uparrow\downarrow\rangle\}$, $\{|\downarrow\Uparrow\uparrow\rangle, |\leftrightharpoons\Downarrow\uparrow\rangle, |\leftrightharpoons\Uparrow\downarrow\rangle, |\uparrow\Downarrow\downarrow\rangle\}$, $\{|\downarrow\Downarrow\uparrow\rangle, |\downarrow\Uparrow\downarrow\rangle, |\leftrightharpoons\Downarrow\downarrow\rangle\}$, and $|\downarrow\Downarrow\downarrow\rangle$. After a suitable shift of the energy scale, the Hamiltonian for the four-dimensional sub-space can be written as

$$\hat{H}^{4D}_{SOHF} = \hbar \begin{bmatrix} (a-b)/2 & \sqrt{2}b/2 & 0 & 0 \\ \sqrt{2}b/2 & -\omega_0/2 & a/2 & 0 \\ 0 & a/2 & \omega_0/2 & \sqrt{2}b/2 \\ 0 & 0 & \sqrt{2}b/2 & (a-b)/2 \end{bmatrix}. \tag{8}$$

An exact, analytical solution for $\hat{H}^{4D}_{SOHF}$ is, to the best of our knowledge, not known. We will be interested in a solution for the case $b \gg a$. At first thought one may speculate that the small a coupling constant merely leads to a small renormalization of the spin dynamics induced by the much larger b, i.e., to a small widening of the Lorentzian cones to yield a width [see Eq. (6)] of $\sqrt{8}b + O(a) \approx \sqrt{8}b$. However, closer inspection of Eq. (8) shows that this is not necessarily the case. This is because b couples levels that are significantly split already at zero field, whereas a couples two subspaces that are degenerate at $\omega_0=0$. Therefore, a may make a much greater contribution to the spin dynamics than expected, unless fields $\omega_0 \gg a$ are applied that lift this degeneracy. Since $b \gg a$ we use first-order time-dependent perturbation theory to study the spin dynamics induced by a. For simplicity we will restrict ourselves to studying the effect of the perturbation to a single initial state only. A complete, quantitative theory is beyond the scope of this paper. In particular we used the following procedure. (i) We calculated the eigenstates and eigenvalues of the zero-order Hamiltonian to first order in ω_0. (ii) We expressed the initial state $|\downarrow\Uparrow\uparrow>$ as a linear combination of zero-order eigenstates. (iii) We used standard first-order time-dependent perturbation theory to obtain the time evolution of this state. (iv) We calculated the time average of the S_z expectation value. We obtain the result

$$\overline{S_z} = \frac{(\omega_0 + b)^2}{(\omega_0 + b)^2 + 8b^2} - \frac{5}{72} \frac{a^2}{\omega_0^2}. \tag{9}$$

Equation (9) shows that the correction diverges for small ω_0 because of the degeneracy of the two subspaces coupled by a. To deal with this divergence we performed a second perturbation calculation, now using ω_0 rather than a as the perturbation. We obtain

$$\overline{S_z} = \frac{1}{16}\frac{\omega_0^2}{a^2}. \tag{10}$$

Furthermore, the expression

$$\overline{S_z} = \frac{(\omega_0+b)^2}{(\omega_0+b)^2+8b^2} - \frac{4}{27}\frac{a^2}{\omega_0^2+\frac{4}{3}a^2} \tag{11}$$

gives an accurate interpolation to the two perturbation expansions. After averaging the zero-order solution over all initial conditions we obtain

$$\overline{S_z} = \frac{9}{10}\frac{\omega_0^2}{\omega_0^2+8b^2} + \frac{1}{10}\frac{\omega_0^2}{ega_0^2+\frac{4}{3}a^2}. \tag{12}$$

For the three-dimensional subspaces one can readily show that also the levels coupled by a are nondegenerate at zero applied field. In this case, we therefore expect that a merely leads to a weak renormalization of the coupling strength. We expect that a full averaging over all initial conditions and subspaces will primarily lead to different numerical values for the coefficients in front of the two Lorentzians, rather than any qualitatively new behavior.

3. Summary of theoretical part

We have studied the combined effect of hyperfine and strong spin-orbit coupling on spin dynamics. As expected, the stronger spin-orbit coupling dominates the behavior, and we expect broad magnetic field effect traces. However, we have shown that a small cone remains at zero field with a width equal to the hyperfine coupling strength. This cone is much smaller than for the case with weak spin-orbit coupling: our calculations estimate a one to two orders of magnitude reduction. The cones for hyperfine interaction and spin-orbit coupling have the same sign because both a and b coupling lead to an increase in spin dynamics and therefore to a reduced time average for S_z.

C. Comparison of theoretical and experimental results

In agreement with theory, the experimental data of Fig. 3 show that the OMAR effect consists of two cones, a low-field cone of a width similar to the hyperfine interaction, superimposed on a second cone that is much wider. The solid lines in Fig. 3 are fits to such a superposition of two cones, namely,

$$\Delta I/I = A_0\frac{B^2}{B^2+B_0^2} + A_1\frac{B^2}{(|B|+B_1)^2}, \tag{13}$$

where we have taken into account the experimental fact that the cones can be of the form either $B^2/(B^2+B_0^2)$ or $B^2/(|B|+B_1)^2$. The fitting results are shown in Table II. Let us first note agreement between model and experiment. (i) The width of the low-field cone is roughly equal to that in materials with small spin-orbit coupling, i.e., $B_0 \approx 5$ mT. (ii) The magnitude of the low-field cone is suppressed by approximately two orders of magnitude compared to results in Alq_3 (see Fig. 2), a material similar to $Ir(ppy)_3$, but without spin-orbit coupling. (iii) The high-field cone widths coincide reasonably well with B_{ISC} from Table I, except for the 10 K data. However, we believe that this deviation may be an artifact due to uncertainty of this particular fit. Indeed, in the control experiment described in Sec. III B in an $Ir(ppy)_3$ device without PEDOT we obtained a fitting result of approx. 100 mT at 10 K also. Several disagreements are, however, also evident. (i) Even the high-field cone does not reach a magnitude similar to that of Alq_3. This is unexpected, since upon applying $B > B_{ISC}$ the spins are pinned by the Zeeman term, and spin-orbit coupling is effectively turned off. One possible explanation is that our extrapolation from the studied magnetic field range (which was limited because of the modulation technique employed) to the final saturation value (i.e., the value A_1, Table II) is seriously off, e.g., because the b coupling is dispersive, or because the saturation behavior is not accurately described by our fitting formula. Another possibility is that OMAR in $Ir(ppy)_3$ is intrinsically much smaller than in Alq_3 despite their similar chemical structure. Future high-field OMAR experiments will address this issue. We note, however, that a quite large effect ($\approx 6\%$), detected through electrophosphorescence measurements in $Ir(ppy)_3$ containing devices at applied field $B=500$ mT was observed by Kalinowski *et al.*[19] (ii) A_0 is temperature dependent, whereas the theory does not include temperature. This, however, is not unexpected: one has to remember that spin dynamics is only part of a complete model of OMAR. The complete theory must describe how the spin dynamics affects the device resistance. Indeed, two such theories have been developed very recently.[6,9] Whereas the reader is referred to these works for a complete discussion, in short, these models are based on a competition between spin dynamics and pair recombination and hopping rate, respectively, and the temperature dependence enters through these rates. The temperature dependence is felt by A_0 since it is the weaker of the two spin coupling processes. (iii) Theory predicts that A_0 and A_1 should have equal signs. We presently do not have an explanation for this serious discrepancy, but note that, to the best of our understanding, the varying signs of experimental OMAR traces, which depend on temperature and applied voltage, remain difficult to understand even in the two OMAR theories that were proposed recently.[6,9]

TABLE II. Values for the fitting parameters for $Ir(ppy)_3$ appearing in Eq. (13).

Temperature (K)	A_0	B_0 (mt)	A_1	B_1 (mt)
300	2×10^{-4}	5.4	-4×10^{-3}	108
200	310^{-4}	4.4	-3.5×10^{-3}	78
100	8×10^{-4}	6.9	-3×10^{-3}	73
10	4×10^{-3}	9.5	-2.5×10^{-3}	28

V. CONCLUSION

We have studied OMAR in Alq_3 and $Ir(ppy)_3$ devices. These materials have similar chemical structures except that the latter contains a heavy atom to enhance spin-orbit coupling. We used fluorescence and phosphorescence spectroscopy to estimate the spin-orbit coupling strength (and the corresponding Zeeman field B_{ISC}) from the measured spectra. A modulation technique was needed to record OMAR traces in the material with strong spin-orbit coupling, since the OMAR effect in $Ir(ppy)_3$ was found to be two orders weaker than in the related Alq_3. It was also evident that the OMAR traces in $Ir(ppy)_3$ comprise a low-field and a high-field effect of opposite signs. Therefore there are at least two relevant coupling strengths in materials with strong spin-orbit coupling, in contrast to Alq_3, where only a single coupling strength was evident. The second coupling strength in $Ir(ppy)_3$ was assigned to spin-orbit coupling.

We compared these experimental results to our theoretical treatment of spin dynamics induced by hyperfine and spin-orbit coupling based on first-order time-dependent perturbation theory. We found, as expected, that the stronger spin-orbit coupling dominates the behavior, predicting magnetic field effect traces that are much wider than those in ordinary organics. However, we have shown that a small cone remains at zero field with a width equal to the hyperfine coupling strength. We believe that this result may serve as a benchmark for the hypothesis that OMAR is related to spin dynamics. Altogether, we believe we have presented strong evidence in support of the notion that OMAR is caused by spin dynamics.

ACKNOWLEDGMENT

This work was supported by NSF Grant No. ECS 04-23911.

*Electronic address: markus-wohlgenannt@uiowa.edu

[1] T. L. Francis, O. Mermer, G. Veeraraghavan, and M. Wohlgenannt, New J. Phys. **6**, 185 (2004).
[2] O. Mermer, G. Veeraraghavan, T. Francis, and M. Wohlgenannt, Solid State Commun. **134**, 631 (2005).
[3] O. Mermer, G. Veeraraghavan, T. L. Francis, Y. Sheng, D. T. Nguyen, M. Wohlgenannt, A. Kohler, M. Al-Suti, and M. Khan, Phys. Rev. B **72**, 205202 (2005).
[4] Y. Yoshida, A. Fujii, M. Ozaki, K. Yoshino, and E. L. Frankevich, Mol. Cryst. Liq. Cryst. **426**, 19 (2005).
[5] C. Garditz, A. G. Muckl, and M. Colle, J. Appl. Phys. **98**, 104507 (2005).
[6] V. Prigodin, J. Bergeson, D. Lincoln, and A. Epstein, Synth. Met. **156**, 757 (2006).
[7] R. Xu, A. Husmann, T. F. Rosenbaum, M.-L. Saboungi, J. E. Enderby, and P. B. Littlewood, Nature (London) **390**, 57 (1997).
[8] C. L. Chien, F. Y. Yang, K. Liu, D. H. Reich, and P. C. Searson, J. Appl. Phys. **87**, 4659 (2000).
[9] M. Wohlgenannt, cond-mat/0609592 (unpublished).
[10] S. Solin, T. Thio, D. R. Hines, and J. J. Heremans, Science **289**, 1530 (2000).
[11] A. L. Efros and B. I. Shklovskii, *Electronic Properties of Doped Semiconductors* (Springer-Verlag, Berlin, 1984).
[12] G. Bergmann, Phys. Rev. Lett. **49**, 162 (1982).
[13] Y. Wu and B. Hu, Appl. Phys. Lett. **89**, 203510 (2006).
[14] Y. Sheng, D. T. Nguyen, G. Veeraraghavan, O. Mermer, M. Wohlgenannt, S. Qiu, and U. Scherf, Phys. Rev. B **74**, 045213 (2006).
[15] M. A. Baldo, M. E. Thompson, and S. R. Forrest, Nature (London) **403**, 750 (2000).
[16] W. J. Finkenzeller and H. Yersin, Chem. Phys. Lett. **377**, 299 (2003).
[17] Y. Kawamura, K. Goushi, J. Brooks, J. J. Brown, H. Sasabe, and C. Adachi, Appl. Phys. Lett. **86**, 071104 (2005).
[18] I. Sokolik, R. Priestley, A. D. Walser, R. Dorsinville, and C. W. Tang, Appl. Phys. Lett. **69**, 4168 (1996).
[19] J. Kalinowski, M. Cocchi, D. Virgili, V. Fattori, and P. Di Marco, Phys. Rev. B **70**, 205303 (2004).
[20] We note that k_{ISC} measured in excitons is actually a lower-limit estimate of the spin-orbit coupling strength that occurs in individual charges or uncorrelated polaron pairs, since in excitons there are additional energy-conservation requirements brought about by exchange interaction.